Finite deformation analysis of hard-magnetic soft materials based on micropolar continuum theory

Farzam Dadgar-Rad[a], Mokarram Hossain[b,*]

[a] *Faculty of Mechanical Engineering, University of Guilan, Rasht, Iran*
[b] *Zienkiewicz Centre for Computational Engineering, College of Engineering, Swansea University, SA1 8EN, UK*

Abstract

Hard-magnetic soft materials (HMSMs), as a sub-class of magneto-active polymers, consist of a polymeric matrix filled with particles of high remnant magnetic induction. The application of external magnetic flux on HMSMs induces a moment on its material particles. From the angular momentum balance law, it is deduced that the Cauchy stress tensor in these materials cannot be symmetric. Therefore, the micropolar continuum theory, with inherent asymmetric stress tensor, is a rational candidate for modeling the deformation of these materials. In the present contribution, an HMSM is modeled as a three-dimensional micropolar continuum body, which is subjected to external magnetic stimuli. The moment resulting from the interaction of the internal and external magnetic fluxes plays the role of a body couple in the micropolar formulation. After developing the main formulation, due to the highly nonlinear nature of the governing equations, the weak form of the equations and its linearization to perform numerical simulations is presented. To demonstrate the capability and performance of the developed formulations, several examples are provided. It is shown that the present formulation can successfully predict the deformation of HMSMs under various loading and boundary conditions.

Keywords: Hard-magnetic soft materials, Micropolar continuum, Magneto-elasticity, Finite element method

*Corresponding author.
Email addresses: dadgar@guilan.ac.ir (Farzam Dadgar-Rad), mokarram.hossain@swansea.ac.uk (Mokarram Hossain)

1. Introduction

Magneto-active polymers (MAPs), as a subgroup of magneto-rheological elastomers (MREs), are a class of smart materials that consist of magnetizable particles embedded into an elastomeric matrix and undergo large mechanical deformations when subject to magnetic loading. These materials can be used in, e.g., soft and flexible electronics, sensors, actuators, soft robots, and vibration absorbers (Bastola and Hossain, 2021; Böse, 2007; Boczkowska and Awietjan, 2009; Bica, 2012; Ivaneyko et al., 2012; Lucarini et al., 2022; Hu et al., 2018; Ren et al., 2019; Yarali et al., 2022; Wu et al., 2020). Due to the importance of these materials in modern applications, it is of particular importance to develop proper theoretical formulations for predicting their deformations, which helps engineers for optimum and effective design of various devices made of MAPs.

Depending on the type of field-responsive magnetic particles, two sub-classes, known as *magnetically-soft MAPs* and *magnetically-hard soft materials* (MHSMs), have been manufactured. The former subclass is composed of particles with low coercivity, namely their magnetization vector changes by applying external magnetic flux. A huge amount of research works on the mathematical formulation and constitutive modeling of these materials, particularly, in the past two decades (e.g., Dorfmann and Ogden (2004), Saxena et al. (2013), Ethiraj and Miehe (2016), Mehnert et al. (2017), Mukherjee et al. (2020), Zabihyan et al. (2020), Bustamante et al. (2021), Hu et al. (2022)). The latter subclass consists of particles, such as $CoFe_2O_4$ or NdFeB, that exhibit considerably large coercivity, so that their magnetization vector remains constant for a wide range of magnetic stimuli (Zhao et al., 2019; Schümann et al., 2020; Lee et al., 2020). Besides this property, the 3D printing technologies allow one to program the local orientation of the magnetized particles. Therefore, HMSMs can experience quick and complex large deformations under relatively small values of external magnetic induction (Lum et al., 2016; Kim et al., 2018; Wu et al., 2019; Alapan et al., 2020; Kuang et al., 2021; Wang et al., 2021; Wu et al., 2021; Yan et al., 2021).

In recent years, a flood of research articles on the theoretical modeling of HMSMs has been published. Some of the most notable articles are cited here. Continuum theories for the elastic deformation of HMSMs have been developed by Kalina et al. (2017) and Zhao et al. (2019) while their viscoelastic effects have been proposed in Garcia-Gonzalez (2019) and Mukherjee et

al. (2021). In contrast to the aforementioned continuum-based macroscopic models, micromechanical and lattice models have been investigated by Zhang et al. (2020), Garcia-Gonzalez and Hossain (2021a,b), and Ye et al. (2021). Moreover, some research works have focused on the finite elastic deformation analysis of two- and three-dimensional beams made of HMSMs, e.g., Wang et al. (2020), Wang et al. (2021), Chen and Wang (2020), Chen et al. (2020a,b), Chen et al. (2021), Rajan and Arockiarajan (2021), Sano et al. (2021), and Yan et al. (2021).

An important property to be pointed out is that the interaction between residual and external magnetic fluxes induces a body couple on the continuum body (e.g., Dorfmann and Ogden (2014)). On the other hand, it is a well-known result from the angular momentum balance law that the Cauchy stress tensor cannot be symmetric in the presence of body couples. A natural conclusion is that the Cauchy stress in HMSMs is asymmetric, see Zhao et al. (2019). Therefore, for the theoretical formulation of HMSMs, it is logical to employ a generalized continuum theory that takes into account the asymmetry of the Cauchy stress. Definitely, *micropolar* and *couple stress* continuum theories are two natural candidates for this purpose. It is known that the couple stress theory leads to higher-order derivatives of the displacement field, and hence, requires C^1 continuity of interpolation functions in a standard finite element (FE) formulation. However, micropolar continuum theory, despite adding additional degrees of freedom (DOFs), can be tackled by C^0-continuous functions (e.g., Ramezani et al. (2008, 2009)). Accordingly, the main purpose of this work is to develop a formulation that models the finite deformation of continuum bodies made of HMSMs based on micropolar theory.

Mathematical foundations of the micropolar continuum theory have been laid down by Eringen and his coworkers (e.g., Kafadar and Eringen (1971), Eringen and Kafadar (1976), Eringen (1999)). In micropolar continuum theory, each material particle is associated with a microstructure that can undergo only rigid rotations independently from the surrounding medium. Therefore, each particle contains six degrees of freedom, three translational which are assigned to the macro-element, and three rotational ones which are referred to the micro-structure. From the kinetic point of view, the interaction between two adjacent surface elements is considered via a couple vector in addition to the traditional traction vector, which leads to the definition of couple stress tensor (e.g., Eringen (1999)). The micropolar theory has been successfully used in modeling the elastoplastic deformation patterns obeys a highly localized zone (e.g., Stein-

mann and Willam (1991); Borst (1993); Iordache and Willam (1998); Tejchman and Wu (2007). Modern formulations of the micropolar elastoplasticity have been developed by, e.g., Steinmann (1994), Grammenoudis and Tsakmakis (2001, 2007), Grammenoudis et al. (2007), Bauer et al. (2012a), and Altenbach and Eremeyev (2014). Moreover, numerical formulations for the finite elastic deformation of micropolar media have been provided by Bauer et al. (2010, 2012b) and Erdelj et al. (2020). The micropolar continuum theory has been also used to formulate crystal plasticity (Mayeur et al., 2011), chiral auxetic lattices (Spadoni and Ruzzene, 2012), vertebral trabecular bone (Goda et al., 2014), lattice structures (Yoder et al., 2018), phononic crystals (Guarín-Zapata et al., 2020), and phase field fracture mechanics (Suh et al., 2020). Furthermore, micropolar formulations of the peridynamic theory have been developed for describing the localized deformations and the fracture of brittle and quasi-brittle materials (Chowdhury et al., 2015; Yu and Chen, 2021).

Zhao et al. (2019) has also pointed out that the optimal effective media for a magnetically responsive material, such as HMSMs, may be polar media. However, they state that further experiments are required to see if size-effects are observed or whether a more complex non-classical continuum is necessary. It is noted that the constitutive equation for stress tensor in Zhao et al. (2019) is a function of external magnetic load. In traditional continuum formulations, at the constitutive level, the stress tensor is a function of kinematic tensors rather than external loads. In this work, it is shown that, due to the dependency of the stress tensor on external magnetic load, their theory cannot solve the problems in which the residual and external magnetic inductions are constant vectors and the boundaries are fixed. Therefore, the main objective of this work is to develop a novel formulation, in the micropolar framework, that can capture the deformation of HMSMs for all types of loading and boundary conditions. Moreover, the dependency of the constitutive equation of stress on the external loading is circumvented. Furthermore, the present research demonstrates a new application of the micropolar continuum theory, namely predicting the deformation of HMSMs as an important class of smart materials.

This paper is structured as follows: In Section 2, the basic properties of hard-magnetic soft materials are introduced. In Section 3, the kinematics, kinetics, linear momentum, and angular momentum balance equations of micropolar continua are presented. In Section 4, the variational formulation of the problem and the corresponding linearization are developed. To

assess the capability and performance of the developed formulation, several numerical examples are provided in Section 5. Finally, the paper is closed with some concluding remarks in Section 6.

Notation: Throughout this work, all lower-case and upper-case Latin indices range over $\{1,2,3\}$. The summation convention holds over all repeated Latin indices. The notations $\mathbf{R}^{\top}$, $\operatorname{tr}\mathbf{R}$, $\det\mathbf{R}$ and $\mathbf{R}^{-1}$ are the transpose, trace, determinant and inverse of the second-order tensor $\mathbf{R}$. For the two second-order tensors $\mathbf{R}$ and $\mathbf{S}$, the fourth-order tensors $\boldsymbol{\mathcal{A}}=\mathbf{R}\otimes\mathbf{S}$, $\boldsymbol{\mathcal{B}}=\mathbf{R}\odot\mathbf{S}$, and $\boldsymbol{\mathcal{C}}=\mathbf{R}\boxtimes\mathbf{S}$ are defined so that their components are given by $\mathcal{A}_{ijkl}=R_{ij}S_{kl}$, $\mathcal{B}_{ijkl}=R_{ik}S_{jl}$, and $\mathcal{C}_{ijkl}=R_{il}S_{kj}$, respectively. The double contraction operation on tensors of different orders is defined by $\mathbf{R}\cdot\mathbf{S}=R_{ij}S_{ij}$ and $(\boldsymbol{\mathcal{A}}\cdot\mathbf{R})_{ij}=\mathcal{A}_{ijpq}R_{pq}$. Two coincided, fixed, Cartesian coordinate systems $\{X_1,X_2,X_3\}$ and $\{x_1,x_2,x_3\}$, with the associated basis vectors $\{\mathbb{e}_1,\mathbb{e}_2,\mathbb{e}_3\}$ and $\{\mathbb{E}_1,\mathbb{E}_2,\mathbb{E}_3\}$, to describe, respectively, the material and spatial quantities are considered. The standard *right gradient* and *right divergence* operators, namely $\operatorname{Grad}\{\bullet\}=\frac{\partial\{\bullet\}}{\partial X_I}\otimes\mathbb{E}_I$, $\operatorname{Div}\{\bullet\}=\frac{\partial\{\bullet\}}{\partial X_I}\cdot\mathbb{E}_I$, $\operatorname{grad}\{\bullet\}=\frac{\partial\{\bullet\}}{\partial x_i}\otimes\mathbb{e}_i$, $\operatorname{div}\{\bullet\}=\frac{\partial\{\bullet\}}{\partial x_i}\cdot\mathbb{e}_i$ are employed in this work.

2. Basic relations of hard-magnetic soft materials under magnetic loading

A body made of hard-magnetic soft materials is modeled as a (micropolar) continuum body in this work. As usual, the notations $\mathcal{B}_0$ and $\mathcal{B}$ denote the reference and current configurations of the body at the times $t=0$ and $t>0$, respectively. At each material point in $\mathcal{B}_0$, a macro-element with center at $\mathbb{X}$ is considered, which is mapped to the new position vector $\mathbb{x}$ as the center of the deformed macro-element in $\mathcal{B}$ via the bijective deformation $\boldsymbol{\phi}$, namely $\mathbb{x}=\boldsymbol{\phi}(\mathbb{X},t)$. Local deformation of the macro-element is governed by the deformation gradient tensor

$$\mathbf{F}=\operatorname{Grad}\boldsymbol{\phi}=\mathbf{I}+\operatorname{Grad}\mathbb{u}=x_{i,I}\mathbb{e}_i\otimes\mathbb{E}_I,\quad J=\det\mathbf{F}>0, \tag{1}$$

where $\mathbb{u}=\mathbb{x}-\mathbb{X}$ is the macro-displacement field, a comma followed by an index denotes differentiation with respect to the coordinates, and $\mathbf{I}$ is the identity tensor.

The residual magnetic flux density at the reference and current configurations are denoted by $\tilde{\mathbb{B}}^{\mathrm{r}}$ and $\mathbb{B}^{\mathrm{r}}$, respectively. The relations between $\tilde{\mathbb{B}}^{\mathrm{r}}$ and $\mathbb{B}^{\mathrm{r}}$ are as follows (Zhao et al., 2019):

$$\mathbb{B}^{\mathrm{r}}=J^{-1}\mathbf{F}\tilde{\mathbb{B}}^{\mathrm{r}}\quad\text{or}\quad\tilde{\mathbb{B}}^{\mathrm{r}}=J\mathbf{F}^{-1}\mathbb{B}^{\mathrm{r}}. \tag{2}$$

The external magnetic flux density $\mathbb{B}^{\mathrm{ext}}$ is applied to the body. At each material point, the interaction between $\mathbb{B}^{\mathrm{ext}}$ and $\mathbb{B}^{\mathrm{r}}$ manifests itself as a body couple exerted on the material points.

The magnetic body couple per unit current volume $\mathbb{c}$, and the magnetic body couple per unit reference volume $\mathbb{c}^\star$ are given by

$$\mathbb{c} = \frac{1}{\mu_0}\mathbb{B}^{\rm r} \times \mathbb{B}^{\rm ext} = \frac{1}{\mu_0} J^{-1}(\mathbf{F}\tilde{\mathbb{B}}^{\rm r}) \times \mathbb{B}^{\rm ext}, \quad \mathbb{c}^\star = J\mathbb{c} = \frac{1}{\mu_0}(\mathbf{F}\tilde{\mathbb{B}}^{\rm r}) \times \mathbb{B}^{\rm ext}, \tag{3}$$

where $\mu_0 = 4\pi \times 10^{-7}\frac{N}{A^2}$ is the magnetic permeability of the free space. It is known that the presence of body couples on a continuum body results in an asymmetric Cauchy stress tensor. Accordingly, from Eq. (3), the existence of body couple in HMSMs is the main motivation of the present research to use the micropolar continuum theory for the deformation analysis of this class of smart and active materials.

Following Zhao et al. (2019) and Chen et al. (2020a,b), it is assumed that the external magnetic flux density is uniform in space. Under this assumption, Zhao et al. (2019) showed that the Maxwell equations of the form (e.g., Dorfmann and Ogden (2014))

$$\mathrm{Curl}\mathbb{H} = \mathbf{0}, \quad \mathrm{Div}\mathbb{B} = 0, \tag{4}$$

are satisfied in HMSMs. Here, $\mathbb{H}$ and $\mathbb{B}$ are the referential magnetic field and the magnetic flux density, respectively. Moreover, "Curl" is the curl operator in the reference configuration.

3. Kinematics and kinetics of micropolar media

In this section, some basic relations of the micropolar continuum theory are presented. For more details and discussions, the fundamental works of Eringen and Kafadar (1976), Eringen (1999), and Steinmann (1994) are suggested.

3.1. Basic kinematic quantities

As was mentioned in the previous section, the local deformation of a macro-element is described by the deformation gradient tensor $\mathbf{F}$ given in Eq. (1). In the micropolar continuum theory, a micro-structure inside each macro-element is considered, which can undergo independent rigid rotations, which is denoted here by the pseudo-vector field $\boldsymbol{\theta}$. The relation between $\boldsymbol{\theta}$ and its corresponding skew-symmetric tensor $\boldsymbol{\Theta}$ is as follows:

$$\boldsymbol{\Theta} = \mathrm{spn}\,\boldsymbol{\theta} = -\boldsymbol{\mathcal{E}}\boldsymbol{\theta}, \quad \boldsymbol{\theta} = \mathrm{axl}\,\boldsymbol{\Theta} = -\frac{1}{2}\boldsymbol{\mathcal{E}}:\boldsymbol{\Theta}, \quad \Theta_{ij} = -\epsilon_{ijk}\theta_k, \quad \theta_i = -\frac{1}{2}\epsilon_{ijk}\Theta_{jk}, \tag{5}$$

where $\boldsymbol{\mathcal{E}}$ is the alternating symbol and ϵ_{ijk} are its components. Using the Euler–Rodriguez formula, the finite micro-rotation tensor $\tilde{\mathbf{R}}$ corresponding to $\boldsymbol{\theta}$ is given by (e.g., Steinmann (1994), Ramezani et al. (2009))

$$\tilde{\mathbf{R}} = \exp \boldsymbol{\Theta} = \cos\theta \mathbf{I} + \frac{\sin\theta}{\theta}\boldsymbol{\Theta} + \frac{1-\cos\theta}{\theta^2}\boldsymbol{\theta}\otimes\boldsymbol{\theta} = \mathbf{I} + \frac{\sin\theta}{\theta}\boldsymbol{\Theta} + \frac{1-\cos\theta}{\theta^2}\boldsymbol{\Theta}^2, \tag{6}$$

where θ is the magnitude of the rotation pseudo-vector $\boldsymbol{\theta}$.

From the polar decomposition theorem, the deformation gradient tensor is uniquely decomposed as $\mathbf{F} = \mathbf{RU} = \mathbf{VR}$. Here, $\mathbf{U}$ is the right stretch, $\mathbf{V}$ is the left stretch, and $\mathbf{R}$ is the macro-rotation tensor. Motivated by the classical polar decomposition, in the micropolar continuum theory the deformation gradient may be decomposed as $\mathbf{F} = \tilde{\mathbf{R}}\tilde{\mathbf{U}} = \tilde{\mathbf{V}}\tilde{\mathbf{R}}$. Accordingly, the micropolar deformation measures $\tilde{\mathbf{U}}$ and $\tilde{\mathbf{V}}$ are defined as follows (e.g., Steinmann (1994)):

$$\tilde{\mathbf{U}} = \tilde{\mathbf{R}}^{\top}\mathbf{F}, \quad \tilde{\mathbf{V}} = \mathbf{F}\tilde{\mathbf{R}}^{\top}, \quad \tilde{U}_{IJ} = \tilde{R}_{nI}F_{nJ}, \quad \tilde{V}_{ij} = F_{iN}\tilde{R}_{jN}, \quad \det\tilde{\mathbf{U}} = \det\tilde{\mathbf{V}} = J. \tag{7}$$

REMARK. It is noted that the right and left stretch tensors $\mathbf{U}$ and $\mathbf{V}$ resulting from the classical polar decomposition of the deformation gradient tensor $\mathbf{F}$ are both symmetric. However, the micropolar deformation tensors $\tilde{\mathbf{U}}$ and $\tilde{\mathbf{V}}$ defined in Eq. (7) are not symmetric, in general. Basically, $\tilde{\mathbf{U}}$ and $\tilde{\mathbf{V}}$ coincide, respectively, with the classical stretch tensors $\mathbf{U}$ and $\mathbf{V}$, if the micro-rotation tensor $\tilde{\mathbf{R}}$ and the macro-rotation $\mathbf{R}$ are identical. As is described in the next subsection, the stress tensor in micropolar theory is also asymmetric, in general. From the constitutive point of view, the stress tensor depends on $\tilde{\mathbf{U}}$ and $\tilde{\mathbf{V}}$ in material and spatial formulations, respectively. Therefore, the asymmetry of $\tilde{\mathbf{U}}$ and $\tilde{\mathbf{V}}$ leads to the asymmetry of the micropolar stress measures in constitutive equations.

In addition to the deformation measures $\tilde{\mathbf{U}}$ and $\tilde{\mathbf{V}}$, the material and spacial wryness tensors, denoted respectively by $\boldsymbol{\Gamma}$ and $\boldsymbol{\gamma}$, are defined by (Eringen and Kafadar, 1976; Pietraszkiewicz and Eremeyev, 2009)

$$\boldsymbol{\Gamma} = -\frac{1}{2}\boldsymbol{\mathcal{E}} : (\tilde{\mathbf{R}}^{\top}\mathrm{Grad}\,\tilde{\mathbf{R}}), \quad \boldsymbol{\gamma} = \tilde{\mathbf{R}}\boldsymbol{\Gamma}\tilde{\mathbf{R}}^{\top}, \quad \Gamma_{IJ} = -\frac{1}{2}\epsilon_{IKL}\tilde{R}_{iK}\tilde{R}_{iL,J}. \tag{8}$$

It is noted that the relation $\mathbf{F} = \mathbf{I} + \mathrm{Grad}\,\mathbb{u}$ holds true for both finite and infinitesimal regimes of deformation. On the other hand, a single coordinate system, say $\{x_1, x_2, x_3\}$, is sufficient to

describe the small deformations of a continuum body. Therefore, for infinitesimal deformations, the deformation gradient $\mathbf{F}$ and the micro-rotation tensor $\tilde{\mathbf{R}}$ may be written as

$$\mathbf{F}_{\text{inf}} = \mathbf{I} + \operatorname{grad} \mathbb{u}, \quad \tilde{\mathbf{R}}_{\text{inf}} = \mathbf{I} + \boldsymbol{\Theta}, \tag{9}$$

where the abbreviation "inf" stands for the infinitesimal. Accordingly, from Eqs. (7)–(9), the infinitesimal micropolar strain $\tilde{\boldsymbol{\varepsilon}}$ and the infinitesimal wryness $\boldsymbol{\kappa}$ are given by

$$\left.\begin{aligned} &\tilde{\boldsymbol{\varepsilon}} = \tilde{\mathbf{U}}_{\text{inf}} - \mathbf{I} = \tilde{\mathbf{V}}_{\text{inf}} - \mathbf{I} = \operatorname{grad} \mathbb{u} - \boldsymbol{\Theta} \quad \text{or} \quad \tilde{\varepsilon}_{ij} = u_{i,j} + \epsilon_{ijk}\theta_k \\ &\boldsymbol{\kappa} = \boldsymbol{\Gamma}_{\text{inf}} = \boldsymbol{\gamma}_{\text{inf}} = \operatorname{grad} \boldsymbol{\theta}, \quad \text{or} \quad \kappa_{ij} = \theta_{i,j} \end{aligned}\right\}. \tag{10}$$

It is noted that $\mathbb{u}$ and $\boldsymbol{\theta}$ and their spatial derivatives are assumed to be sufficiently small in Eqs. (9) and (10).

3.2. Kinetic quantities and balance of linear and angular momentum

In the classical continuum theory, the interaction between two adjacent surface elements is modeled via a traction vector, which is defined as the force per unit area of the elements. In the micropolar theory, a couple vector has been also taken into account. More precisely, an infinitesimal area element $\mathrm{d}\mathcal{S}_0$ with the outward unit normal $\mathbb{N}$ in the reference configuration is considered, which is deformed into the area element $\mathrm{d}\mathcal{S}$ with the outward unit normal $\mathbb{n}$ in the current configuration. The traction vector and the couple vector on $\mathrm{d}\mathcal{S}$ are denoted by $\mathbb{t}^{(\mathbb{n})}$ and $\mathbb{z}^{(\mathbb{n})}$, respectively. There exist the non-symmetric Cauchy stress $\boldsymbol{\sigma} = \sigma_{ij}\mathbb{e}_i \otimes \mathbb{e}_j$ and the couple stress tensor $\mathbf{m} = m_{ij}\mathbb{e}_i \otimes \mathbb{e}_j$ so that the following relations hold:

$$\mathbb{t}^{(\mathbb{n})} = \boldsymbol{\sigma}\mathbb{n}, \quad \mathbb{z}^{(\mathbb{n})} = \mathbf{m}\mathbb{n}, \quad t_i^{(\mathbb{n})} = \sigma_{ij}n_j, \quad z_i^{(\mathbb{n})} = m_{ij}n_j. \tag{11}$$

Similarly, let $\mathbb{T}^{(\mathbb{N})}$ and $\mathbb{Z}^{(\mathbb{N})}$ be, respectively, the traction and couple vectors on the undeformed area element $\mathrm{d}\mathcal{S}_0$. Accordingly, there exist the first Piola–Kirchoff type stress $\mathbf{P} = P_{iJ}\mathbb{e}_i \otimes \mathbb{E}_J$ and the couple stress $\mathbf{M} = M_{iJ}\mathbb{e}_i \otimes \mathbb{E}_J$ with the following properties:

$$\left.\begin{aligned} \mathbb{T}^{(\mathbb{N})} = \mathbf{P}\mathbb{N}, \quad \mathbb{Z}^{(\mathbb{N})} = \mathbf{M}\mathbb{N}, \quad \mathbf{P} = J\boldsymbol{\sigma}\mathbf{F}^{-\top}, \quad \mathbf{M} = J\mathbf{m}\mathbf{F}^{-\top} \\ T_i^{(\mathbb{N})} = P_{iJ}N_J, \quad Z_i^{(\mathbb{N})} = M_{iJ}N_J, \quad P_{iJ} = J\sigma_{ij}X_{J,j}, \quad M_{iJ} = Jm_{ij}X_{J,j} \end{aligned}\right\}. \tag{12}$$

It is emphasized that the index i in $\{\sigma_{ij}, m_{ij}, P_{ij}, M_{ij}\}$ denotes the direction at which the stress/couple stress component acts. Moreover, the indices j or J indicate the *plane* on which

the stress/couple stress component is applied. This is in agreement with the standard notation in the textbooks on continuum mechanics. It is noted that $\boldsymbol{\sigma}$ and $\mathbf{m}$ are spatial tensors, while $\mathbf{P}$ and $\mathbf{M}$ are two-point tensors. For later use, the following stress $\tilde{\mathbf{P}}$ and the couple stress $\tilde{\mathbf{M}}$, which are material tensors, are defined:

$$\tilde{\mathbf{P}} = \tilde{\mathbf{R}}^{\top}\mathbf{P} = J\tilde{\mathbf{R}}^{\top}\boldsymbol{\sigma}\mathbf{F}^{-\top}, \quad \tilde{\mathbf{M}} = \tilde{\mathbf{R}}^{\top}\mathbf{M} = J\tilde{\mathbf{R}}^{\top}\mathbf{m}\mathbf{F}^{-\top}. \tag{13}$$

Next, let $\mathbb{f}$ and $\mathbb{f}^{\star} = J\mathbb{f}$ be the body force per unit current and reference volume, respectively. Similarly, $\mathbb{c}$ and $\mathbb{c}^{\star} = J\mathbb{c}$ are considered to be, respectively, the current and the referential body couples per unit volume. For the case of hard-magnetic soft materials under the magnetic loading described in Section 2, the expressions for $\mathbb{c}$ and $\mathbb{c}^{\star}$ are exactly those given in Eq. (3). By neglecting inertia effects, standard arguments lead to the following expressions for the linear and angular momentum balances in spatial setting:

$$\left.\begin{aligned} \operatorname{div}\boldsymbol{\sigma} + \mathbb{f} = \mathbf{0} \quad \text{or} \quad \sigma_{ij,j} + f_i = 0 \\ \operatorname{div}\mathbf{m} - \boldsymbol{\mathcal{E}}\!:\!\boldsymbol{\sigma} + \mathbb{c} = \mathbf{0} \quad \text{or} \quad m_{ij,j} - \epsilon_{ijk}\sigma_{jk} + c_i = 0 \end{aligned}\right\}. \tag{14}$$

Moreover, the the balance equations in material form are given by

$$\left.\begin{aligned} \operatorname{Div}\mathbf{P} + \mathbb{f}^{\star} = \mathbf{0} \quad \text{or} \quad P_{iJ,J} + f_i^{\star} = 0 \\ \operatorname{Div}\mathbf{M} - \boldsymbol{\mathcal{E}}\!:\!\mathbf{P} + \mathbb{c}^{\star} = \mathbf{0} \quad \text{or} \quad M_{iJ,J} - \epsilon_{ijK}P_{jK} + c_i^{\star} = 0 \end{aligned}\right\}. \tag{15}$$

REMARK. The strain components $\tilde{\varepsilon}_{ij}$ and the wryness ones κ_{ij} in this work are the transpose of those defined by Eringen (e.g., Eringen and Kafadar (1976), Eringen (1999)). However, the mentioned components in this work are, respectively, consistent with the stress and couple stress components σ_{ij} and m_{ij}, so that the pairs $(\tilde{\varepsilon}_{ij}, \sigma_{ij})$ and (κ_{ij}, m_{ij}) are work-conjugate quantities. The definitions of the components of various second-order quantities in this work, besides the standard *right gradient* and *right divergence* operators, circumvent using an extra *transpose* sign in many relations. Moreover, some of the relations, e.g., those in Eq. $(14)_{1,2}$ and $(15)_{1,2}$, will be the same as those frequently used in the classical continuum theory.

4. The weak form and the linearization of equilibrium equations

It is well known that the weak form of the equilibrium equations is equivalent to the *principle of virtual work*, which may be written of the form $\delta\mathcal{U} - \delta\mathcal{W} = 0$ (Wriggers, 2008). Here, $\delta\mathcal{U}$ and

$\delta\mathcal{W}$ are the virtual internal energy and the virtual work of external loads, respectively. In the following subsections, the expressions for $\delta\mathcal{U}$ and $\delta\mathcal{W}$, and their linearization to perform numerical simulations are provided. Additionally, a nonlinear finite element formulation is developed and a simple extension of the neo-Hookean material model to micropolar media is proposed.

4.1. Virtual internal energy and its linearization

Let $\delta\mathbb{u}$ and $\delta\boldsymbol{\theta}$ be the virtual displacement and virtual rotation pseudo-vector, respectively. Using Eqs. (1) and (6), the variations of the deformation gradient tensor $\mathbf{F}$ and the micro-rotation tensor $\tilde{\mathbf{R}}$ may be written as

$$\left.\begin{aligned} \delta\mathbf{F} = \operatorname{Grad}\delta\mathbb{u} = \delta\bar{\mathbf{L}}\mathbf{F} \quad \text{with} \quad \delta\bar{\mathbf{L}} \overset{\text{def}}{=} \operatorname{grad}\delta\mathbb{u} = \frac{\partial\delta u_i}{\partial x_j}\mathbb{e}_i\otimes\mathbb{e}_j \\ \delta\tilde{\mathbf{R}} = \delta\boldsymbol{\Omega}\tilde{\mathbf{R}} \quad \text{with} \quad \delta\boldsymbol{\Omega} = \operatorname{spn}\delta\boldsymbol{\phi} \quad \text{and} \quad \delta\boldsymbol{\phi} = \boldsymbol{\Lambda}\delta\boldsymbol{\theta} \end{aligned}\right\}. \tag{16}$$

Here, $\boldsymbol{\Lambda}$ is the following second-order tensor:

$$\boldsymbol{\Lambda} = \frac{\sin\theta}{\theta}\mathbf{I} - \frac{\cos\theta - 1}{\theta^2}\boldsymbol{\Theta} + \frac{\theta - \sin\theta}{\theta^3}\boldsymbol{\theta}\otimes\boldsymbol{\theta}. \tag{17}$$

It is noted that the definition of $\delta\bar{\mathbf{L}}$ in Eq. $(16)_2$ is similar to the velocity gradient tensor $\mathbf{L} = \operatorname{grad}\dot{\mathbb{u}} = \dot{u}_{i,j}\mathbb{e}_i\otimes\mathbb{e}_j$. From Eqs. $(7)_1$, (8), and (16), it is possible to write the expressions for $\delta\tilde{\mathbf{U}}$ and $\delta\boldsymbol{\Gamma}$ in the following forms:

$$\delta\tilde{\mathbf{U}} = \tilde{\mathbf{R}}^{\top}(\delta\bar{\mathbf{L}} - \delta\boldsymbol{\Omega})\mathbf{F}, \quad \delta\boldsymbol{\Gamma} = \tilde{\mathbf{R}}^{\top}\operatorname{Grad}\delta\boldsymbol{\phi} = \tilde{\mathbf{R}}^{\top}\operatorname{grad}\delta\boldsymbol{\phi}\mathbf{F}. \tag{18}$$

Next, let Ψ be the internal energy per unit reference volume of the micropolar continuum body. The expression for the material time derivative of Ψ for purely mechanical deformations is available in the literature (e.g., Eringen (1999), Ramezani and Naghdabadi (2007)). Following the same lines, the expression for the *virtual* form of Ψ is obtained to be

$$\delta\Psi = J\boldsymbol{\sigma}\colon(\delta\bar{\mathbf{L}} - \delta\boldsymbol{\Omega}) + J\mathbf{m}\colon\operatorname{grad}\delta\boldsymbol{\phi}. \tag{19}$$

In the sequel, it is assumed that the material is hyperelastic. In this case, the internal energy density is of the form $\Psi = \bar{\Psi}(\tilde{\mathbf{U}}, \boldsymbol{\Gamma}) = \hat{\Psi}(\tilde{\mathbf{V}}, \boldsymbol{\gamma})$. The dependency of Ψ to the material tensors $\tilde{\mathbf{U}}$ and $\boldsymbol{\Gamma}$ is of particular interest, which leads to the following expression for the virtual internal energy density:

$$\begin{aligned} \delta\Psi &= \frac{\partial\Psi}{\partial\tilde{\mathbf{U}}}\colon\delta\tilde{\mathbf{U}} + \frac{\partial\psi}{\partial\boldsymbol{\Gamma}}\colon\delta\boldsymbol{\Gamma} \\ &= (\tilde{\mathbf{R}}\frac{\partial\Psi}{\partial\tilde{\mathbf{U}}}\mathbf{F}^{\top})\colon(\delta\bar{\mathbf{L}} - \delta\boldsymbol{\Omega}) + (\tilde{\mathbf{R}}\frac{\partial\Psi}{\partial\boldsymbol{\Gamma}}\mathbf{F}^{\top})\colon\operatorname{grad}\delta\boldsymbol{\phi}, \end{aligned} \tag{20}$$

where use has been made of Eq. (18). By comparing Eqs. (19) and (20), and using Eqs. (12) and (13), the relations between various stress and couple stress measures with the strain energy density function is obtained, namely

$$\{\boldsymbol{\sigma}, \mathbf{P}, \tilde{\mathbf{P}}\} = \left\{\frac{1}{J}\tilde{\mathbf{R}}\frac{\partial \Psi}{\partial \tilde{\mathbf{U}}}\mathbf{F}^{\top}, \tilde{\mathbf{R}}\frac{\partial \Psi}{\partial \tilde{\mathbf{U}}}, \frac{\partial \Psi}{\partial \tilde{\mathbf{U}}}\right\}, \quad \{\mathbf{m}, \mathbf{M}, \tilde{\mathbf{M}}\} = \left\{\frac{1}{J}\tilde{\mathbf{R}}\frac{\partial \Psi}{\partial \boldsymbol{\Gamma}}\mathbf{F}^{\top}, \tilde{\mathbf{R}}\frac{\partial \Psi}{\partial \boldsymbol{\Gamma}}, \frac{\partial \Psi}{\partial \boldsymbol{\Gamma}}\right\}. \tag{21}$$

In particular, in terms of the first Piola–Kirchhoff type stress $\mathbf{P}$ and couple stress $\mathbf{M}$ the expression for $\delta\Psi$ may be rewritten as

$$\delta\Psi = \mathbf{P}\cdot\delta\mathbf{Y}^{(1)} + \mathbf{M}\cdot\delta\mathbf{Y}^{(2)}, \tag{22}$$

where $\delta\mathbf{Y}^{(1)}$ and $\delta\mathbf{Y}^{(2)}$ are defined by

$$\delta\mathbf{Y}^{(1)} \overset{\text{def}}{=} \tilde{\mathbf{R}}\delta\tilde{\mathbf{U}} = \delta\mathbf{F} - \delta\boldsymbol{\Omega}\mathbf{F}, \quad \delta\mathbf{Y}^{(2)} \overset{\text{def}}{=} \tilde{\mathbf{R}}\delta\boldsymbol{\Gamma} = \operatorname{Grad}\delta\boldsymbol{\phi}. \tag{23}$$

To perform numerical simulations, the linearized form of the virtual strain energy density is needed. To do so, it is just sufficient to calculate the increment of $\delta\Psi$ under the incremental displacement $\Delta\mathbb{u}$ and the incremental rotation $\Delta\boldsymbol{\theta}$. From Eqs. (20) and (22), the increment of the virtual strain energy density, $\Delta\delta\Psi$, is calculated as follows:

$$\begin{aligned}\Delta\delta\Psi = {} & \delta\mathbf{Y}^{(1)}\cdot\boldsymbol{\mathcal{A}}^{(1)}\cdot\Delta\mathbf{Y}^{(1)} + \delta\mathbf{Y}^{(2)}\cdot\boldsymbol{\mathcal{A}}^{(2)}\cdot\Delta\mathbf{Y}^{(2)} + \delta\mathbf{Y}^{(1)}\cdot\boldsymbol{\mathcal{A}}^{(3)}\cdot\Delta\mathbf{Y}^{(2)} \\ & + \delta\mathbf{Y}^{(2)}\cdot\boldsymbol{\mathcal{A}}^{(4)}\cdot\Delta\mathbf{Y}^{(1)} + \mathbf{P}\cdot\Delta\delta\mathbf{Q}^{(1)} + \mathbf{M}\cdot\Delta\delta\mathbf{Q}^{(2)}.\end{aligned} \tag{24}$$

Here, the expressions for the incremental quantities, e.g., $\Delta\mathbf{Y}^{(1)}$, are the same as the variational counterparts except that the operator δ is replaced by Δ. Moreover, the components of the fourth-order tensors $\boldsymbol{\mathcal{A}}^{(\alpha)}$ $(\alpha = 1, 2, 3, 4)$ are given by

$$\{\mathcal{A}^{(1)}_{iJkL}, \mathcal{A}^{(2)}_{iJkL}, \mathcal{A}^{(3)}_{iJkL}, \mathcal{A}^{(4)}_{iJkL}\} = \mathcal{R}_{iPkQ}\left\{\frac{\partial^2\Psi}{\partial\tilde{U}_{PJ}\partial\tilde{U}_{QL}}, \frac{\partial^2\Psi}{\partial\Gamma_{PJ}\partial\Gamma_{QL}}, \frac{\partial^2\Psi}{\partial\tilde{U}_{PJ}\partial\Gamma_{QL}}, \frac{\partial^2\Psi}{\partial\Gamma_{PJ}\partial\tilde{U}_{QL}}\right\}, \tag{25}$$

where $\mathcal{R}_{iPkQ} = \tilde{R}_{iP}\tilde{R}_{kQ}$. Furthermore, the quantities denoted by $\Delta\delta\mathbf{Q}^{(1)}$ and $\Delta\delta\mathbf{Q}^{(2)}$ are *defined* as follows:

$$\left.\begin{aligned}\Delta\delta\mathbf{Q}^{(1)} &\overset{\text{def}}{=} \frac{1}{2}[(\Delta\boldsymbol{\Omega}\delta\boldsymbol{\Omega} + \delta\boldsymbol{\Omega}\Delta\boldsymbol{\Omega})\mathbf{F} - 2(\delta\boldsymbol{\Omega}\Delta\mathbf{F} + \Delta\boldsymbol{\Omega}\delta\mathbf{F})] \\ \Delta\delta\mathbf{Q}^{(2)} &\overset{\text{def}}{=} -\frac{1}{2}(\Delta\boldsymbol{\Omega}\operatorname{Grad}\delta\boldsymbol{\phi} + \delta\boldsymbol{\Omega}\operatorname{Grad}\Delta\boldsymbol{\phi})\end{aligned}\right\}. \tag{26}$$

4.2. Virtual work of external magnetic loading and the numerical solution procedure

In this subsection, the expression for the virtual external work, resulting from the external magnetic flux $\mathbb{B}^{\text{ext}}$ on a hard-magnetic soft material, is presented. It was mentioned the body couple per unit reference volume, $\mathbb{c}^{\star}$, is given by Eq. $(3)_2$. Therefore, the virtual work per unit reference volume expended by the external magnetic flux on the continuum body, denoted here by $\delta\Phi$, is given by

$$\delta\Phi = \mathbb{c}^{\star} \cdot \delta\boldsymbol{\theta} = \frac{1}{\mu_0}[(\mathbf{F}\tilde{\mathbb{B}}^{\text{r}}) \times \mathbb{B}^{\text{ext}}] \cdot \delta\boldsymbol{\theta}, \tag{27}$$

indicating that the magnetic body couple $\mathbb{c}^{\star}$ is work-conjugate to the micro-rotation $\boldsymbol{\theta}$. The increment of $\delta\Phi$ is then calculated to be

$$\Delta\delta\Phi = \mathbb{c}^{\star} \cdot \delta\boldsymbol{\theta} = \frac{1}{\mu_0}\delta\boldsymbol{\theta} \cdot [(\Delta\mathbf{F}\tilde{\mathbb{B}}^{\text{r}}) \times \mathbb{B}^{\text{ext}}], \tag{28}$$

from which the components of the load stiffness matrix are extracted.

REMARK. In the present formulation, the magnetic effect is just observed in the virtual external work in Eq. dWext. Therefore, the magnetic and mechanical problems are not coupled. The same holds for the model proposed by Zhao et al. (2019). It has been assumed that due to the large value of the remnant magnetic flux $\tilde{\mathbb{B}}^{\text{r}}$, the change in the magnetic internal energy of HMSMs is negligible. Therefore, an internal energy term involving magnetic effects has not been considered in the formulation. It is also noted that an internal energy term due to magnetic effects plays a crucial role in magnetically-soft materials. However, the comparison of our results with experimental data in Section 5 indicates that such an assumption is acceptable, at least for the cases considered in the present work. On the other hand, if the change in the internal magnetic flux density of the material due to the effect of external magnetic loading is considerable, extra energy density terms due to magnetic effects (similar to magnetically-soft MAPs) have to be added to the mechanical part of the strain energy density function. Extension of the present work to that including internal magnetic energy terms will be made in future contributions.

4.3. Finite element formulation

In this subsection, a nonlinear finite element formulation in the material framework is developed. The displacement and rotation components, over a typical element, are interpolated as

follows:

$$\{u_i, \delta u_i, \Delta u_i\} = \sum_{\alpha=1}^{n_u} N_\alpha \{U_{\alpha i}, \delta U_{\alpha i}, \Delta U_{\alpha i}\}, \quad \{\theta_i, \delta\theta_i, \Delta\theta_i\} = \sum_{\beta=1}^{n_\theta} \bar{N}_\beta \{\tilde{\Theta}_{\beta i}, \delta\tilde{\Theta}_{\beta i}, \Delta\tilde{\Theta}_{\beta i}\}, \tag{29}$$

where n_u and n_θ are the number of nodes with displacement and rotational DOFs, respectively. Moreover, N_α ($\alpha = 1, ..., n_u$) and $\bar{N}_\beta$ ($\beta = 1, ..., n_\theta$) are the interpolation functions. Furthermore, $U_{\alpha i}$ and $\tilde{\Theta}_{\beta i}$ are the nodal values of u_i and θ_i, respectively. By integrating Eqs. (22) and (27) over the reference volume V_0^e of the typical element and using Eqs. (23) and (29), the virtual internal energy of the element, $\delta\mathcal{U}^{\mathfrak{e}}$, and the virtual work of external magnetic loading on the element, $\delta\mathcal{W}^{\mathfrak{e}}$, may be written as

$$\delta\mathcal{U}^{\mathfrak{e}} = \sum_{\alpha=1}^{n_u} F_{\alpha i}^{\mathrm{int}u} \delta U_{\alpha i} + \sum_{\beta=1}^{n_\theta} F_{\beta i}^{\mathrm{int}\theta} \delta\tilde{\Theta}_{\beta i}, \quad \delta\mathcal{W}^{\mathfrak{e}} = \sum_{\beta=1}^{n_\theta} F_{\beta i}^{\mathrm{ext}\theta} \delta\tilde{\Theta}_{\beta i}, \tag{30}$$

where the internal forces $F_{\alpha i}^{\mathrm{int}u}$ and $F_{\beta i}^{\mathrm{int}\theta}$, and the external force $F_{\beta i}^{\mathrm{ext}\theta}$, are defined as follows:

$$\left.\begin{aligned} F_{\alpha i}^{\mathrm{int}u} &= \int_{V_0^e} N_{\alpha,J} P_{iJ} \mathrm{d}V_0^e \\ F_{\beta i}^{\mathrm{int}\theta} &= \int_{V_0^e} [\epsilon_{mkr} \bar{N}_\beta \Lambda_{ri} F_{kJ} P_{mJ} + (\bar{N}_\beta \Lambda_{mi})_{,J} M_{mJ}] \mathrm{d}V_0^e \\ F_{\beta i}^{\mathrm{ext}\theta} &= \frac{1}{\mu_0} \int_{V_0^e} \epsilon_{imj} \bar{N}_\beta F_{mJ} \tilde{B}_J^{\mathrm{r}} B_j^{\mathrm{ext}} \mathrm{d}V_0^e \end{aligned}\right\}. \tag{31}$$

On the other hand, the linearized equilibrium equations resulting from Eq. (24) and (28) may be written as

$$\Delta\delta\mathcal{U}^{\mathfrak{e}} - \Delta\delta\mathcal{W}^{\mathfrak{e}} = -(\delta\mathcal{U}^{\mathfrak{e}} - \delta\mathcal{W}^{\mathfrak{e}}), \tag{32}$$

from which the following system of algebraic equations, for the unknown nodal values of the typical element, is obtained:

$$\begin{cases} \displaystyle\sum_{\alpha=1}^{n_u} K_{\eta j \alpha i}^{(uu)} \Delta U_{\alpha i} + \sum_{\beta=1}^{n_\theta} K_{\eta j \beta i}^{(u\theta)} \Delta\tilde{\Theta}_{\beta i} = -F_{\eta j}^{\mathrm{int}u} \\ \displaystyle\sum_{\alpha=1}^{n_u} K_{\omega j \alpha i}^{(\theta u)} \Delta U_{\alpha i} + \sum_{\beta=1}^{n_\theta} K_{\omega j \beta i}^{(\theta\theta)} \Delta\tilde{\Theta}_{\beta i} = -(F_{\omega j}^{\mathrm{int}\theta} - F_{\omega j}^{\mathrm{ext}\theta}) \end{cases} \tag{33}$$

where the expressions for $K_{\eta j \alpha i}^{(uu)}$, $K_{\eta j \beta i}^{(u\theta)}$, $K_{\omega j \alpha i}^{(\theta u)}$, and $K_{\omega j \beta i}^{(\theta\theta)}$ (with $\alpha, \eta = 1, 2, ..., n_u$ and $\beta, \omega = 1, 2, ..., n_\theta$), are as follows:

$$K_{\eta j \alpha i}^{(uu)} = \int_{V_0^e} N_{\alpha,I} N_{\eta,J} \mathcal{A}_{jJiI}^{(1)} \mathrm{d}V_0^e, \tag{34}$$

$$K^{(u\theta)}_{\eta j\beta i} = \int_{V_0^e} \{N_{\eta,J}[\epsilon_{spq}\Lambda_{qi}\bar{N}_\beta F_{pI}\mathcal{A}^{(1)}_{jJsI} + (\Lambda_{si}\bar{N}_\beta)_{,I}\mathcal{A}^{(3)}_{jJsI}] + \epsilon_{mjp}\Lambda_{pi}N_{\eta,I}\bar{N}_\beta P_{mI}\}\mathrm{d}V_0^e, \tag{35}$$

$$\begin{aligned} K^{(\theta u)}_{\omega j\alpha i} = \int_{V_0^e} [&\epsilon_{mkr}\bar{N}_\omega N_{\alpha,I}\Lambda_{rj}F_{kJ}\mathcal{A}^{(1)}_{mJiI} + N_{\alpha,I}(\Lambda_{mj}\bar{N}_\omega)_{,J}\mathcal{A}^{(4)}_{mJiI} + \epsilon_{mip}\Lambda_{pj}N_{\alpha,I}\bar{N}_\omega P_{mI} \\ &- \frac{1}{\mu_0}\epsilon_{ikj}N_{\alpha,J}\bar{N}_\omega \tilde{B}^{\mathrm{r}}_J B^{\mathrm{ext}}_k]\mathrm{d}V_0^e, \end{aligned} \tag{36}$$

$$\begin{aligned} K^{(\theta\theta)}_{\omega j\beta i} = \int_{V_0^e} \{&\epsilon_{mkr}\epsilon_{spq}\Lambda_{rj}\Lambda_{qi}\bar{N}_\omega\bar{N}_\beta F_{kJ}F_{pI}\mathcal{A}^{(1)}_{mJsI} + (\Lambda_{si}\bar{N}_\beta)_{,I}(\Lambda_{mj}\bar{N}_\omega)_{,J}\mathcal{A}^{(2)}_{mJsI} \\ &+ \epsilon_{mkr}\Lambda_{rj}\bar{N}_\omega F_{kJ}(\Lambda_{si}\bar{N}_\beta)_{,I}\mathcal{A}^{(3)}_{mJsI} + \epsilon_{spq}\Lambda_{qi}\bar{N}_\beta F_{pI}(\Lambda_{mj}\bar{N}_\omega)_{,J}\mathcal{A}^{(4)}_{mJsI} \\ &+ \frac{1}{2}\bar{N}_\omega\bar{N}_\beta P_{mI}F_{rI}(\Lambda_{ri}\Lambda_{mj} + \Lambda_{rj}\Lambda_{mi} - 2\Lambda_{pi}\Lambda_{pj}\delta_{mr}) \\ &+ \frac{1}{2}\epsilon_{mpr}M_{mI}[\Lambda_{ri}\bar{N}_\beta(\Lambda_{pj}\bar{N}_\omega)_{,I} + \Lambda_{rj}\bar{N}_\omega(\Lambda_{pi}\bar{N}_\beta)_{,I}]\}\mathrm{d}V_0^e. \end{aligned} \tag{37}$$

It is noted that the terms containing $\mathcal{A}^{\alpha}_{iIjJ}$ $(\alpha = 1, 2, ..., 4)$ construct the material part of the element stiffness matrix, while the terms having P_{mI} and M_{mI} form the geometric part of it. Moreover, the latest term in Eq. (36) involving B^{ext}_k is the building block of the load stiffness matrix. Finally, the assembled system of equations may be written of the form $\hat{\mathbb{K}}\Delta\hat{\mathbb{U}} = -\hat{\mathbb{R}}$. Here, $\Delta\hat{\mathbb{U}}$ is the incremental generalized displacement vector that contains the nodal incremental displacements and micro-rotations. Moreover, $\hat{\mathbb{K}}$ is the assembled stiffness matrix, and $\hat{\mathbb{R}}$ is the assembled residual vector. After finding $\Delta\hat{\mathbb{U}}$, the displacement vector at a node is updated via the relation $\mathbb{u}+\Delta\mathbb{u} \to \mathbb{u}$. To update the rotation pseudo-vector, it is first noted that the rotation tensor $\tilde{\mathbf{R}}$ corresponding the rotation $\boldsymbol{\theta}$ is given by (e.g., Argyris (1982) and Steinmann (1994))

$$\tilde{\mathbf{R}} = \exp(\mathrm{spn}\,\boldsymbol{\theta}) = \mathbf{I} + \frac{2}{1+\theta^{*2}}(\mathrm{spn}\,\boldsymbol{\theta}^* + \mathrm{spn}^2\boldsymbol{\theta}^*) \quad \text{with} \quad \boldsymbol{\theta}^* = \frac{\boldsymbol{\theta}}{\theta}\tan\frac{\theta}{2}. \tag{38}$$

Here, $\boldsymbol{\theta}^*$ is the normalized rotation pseudo-vector, and $\theta^* = |\boldsymbol{\theta}^*| = \tan\frac{\theta}{2}$. A similar relation holds under the incremental rotation pseudo-vector $\Delta\boldsymbol{\theta}$, and the incremental rotation tensor $\Delta\tilde{\mathbf{R}} = \exp(\mathrm{spn}\,\Delta\boldsymbol{\theta})$ may be defined. It is noted that both $\boldsymbol{\theta}$ and $\Delta\boldsymbol{\theta}$ are described in the $\{x_1, x_2, x_3\}$ coordinate system. The compound rotation tensor is given by $\tilde{\mathbf{R}}_{\mathrm{comp}} = (\Delta\tilde{\mathbf{R}})\tilde{\mathbf{R}}$. However, as has been emphasized by Argyris (1982), it is important to notice that

$$\exp(\mathrm{spn}\,\boldsymbol{\theta})\exp(\mathrm{spn}\,\Delta\boldsymbol{\theta}) \neq \exp(\mathrm{spn}\,\Delta\boldsymbol{\theta})\exp(\mathrm{spn}\,\boldsymbol{\theta}) \neq \exp(\mathrm{spn}\,(\boldsymbol{\theta}+\Delta\boldsymbol{\theta})). \tag{39}$$

As has been proven rigorously by Argyris (1982), the normalized compound rotation pseudo-vector resulting from the two subsequent rotations $\boldsymbol{\theta}$ and $\Delta\boldsymbol{\theta}$ is given by

$$\boldsymbol{\theta}^*_{\text{comp}} = \frac{\boldsymbol{\theta}^* + \Delta\boldsymbol{\theta}^* + (\text{spn}\,\Delta\boldsymbol{\theta}^*)\boldsymbol{\theta}^*}{1 - \boldsymbol{\theta}^* \cdot \Delta\boldsymbol{\theta}^*}, \tag{40}$$

from which the compound rotation $\boldsymbol{\theta}_{\text{comp}}$ is obtained with the aid of Eq. $(38)_2$.

4.4. Micropolar neo-Hookean constitutive model

The theory of constitutive equations for micropolar hyperelastic materials has been developed in the literature (Kafadar and Eringen, 1971; Eringen and Kafadar, 1976; Steinmann, 1994; Eringen, 1999; Ramezani et al., 2009). The purpose of this subsection is to extend the classical neo-Hookean material law to micropolar elasticity. A simple extension with *spatial representation* has been proposed by Ramezani et al. (2009). Here, a similar constitutive equation in *material framework* is developed. To do so, it is first noted that the constitutive equation for the asymmetric stress tensor $\boldsymbol{\sigma}$ in linear elastic isotropic micropolar materials is of the form

$$\boldsymbol{\sigma} = \lambda \text{tr}\,\boldsymbol{\varepsilon} + (\mu + \eta)\boldsymbol{\varepsilon} + (\mu - \eta)\boldsymbol{\varepsilon}^\top, \tag{41}$$

where λ and μ are the usual Lame' constants, and η is a new material parameter. Clearly, by setting $\eta = 0$, the classical generalized Hooke's law for linear isotropic solids is retrieved. Next, the following form for the free energy function per unit reference volume is proposed:

$$\Psi = k_1 \text{tr}\,(\tilde{\mathbf{U}}\tilde{\mathbf{U}}^\top) + k_2 \text{tr}\,(\tilde{\mathbf{U}}^2) + \frac{1}{2}\lambda(\ln J)^2 - \mu \ln J + \frac{1}{2}\mu l^2 \text{tr}\,(\boldsymbol{\Gamma}\boldsymbol{\Gamma}^\top), \tag{42}$$

where k_1 and k_2 are the unknown constants to be determined, and l is a material length-scale parameter. It is first noted that from $\det \tilde{\mathbf{U}} = J$ it follows that $\partial J/\partial \tilde{\mathbf{U}} = J\tilde{\mathbf{U}}^{-\top}$. The material stress $\tilde{\mathbf{P}}$ and the couple stress $\tilde{\mathbf{M}}$ are then calculated to be

$$\tilde{\mathbf{P}} = \frac{\partial \Psi}{\partial \tilde{\mathbf{U}}} = (2k_1 + k_2)\tilde{\mathbf{U}} + k_2\tilde{\mathbf{U}}^\top + (\lambda \ln J - \mu)\tilde{\mathbf{U}}^{-\top}, \quad \tilde{\mathbf{M}} = \frac{\partial \Psi}{\partial \boldsymbol{\Gamma}} = \mu l^2 \boldsymbol{\Gamma}. \tag{43}$$

Next, from Eqs. (9) and (10) it is deduced that the following relations at the infinitesimal regime of deformations hold:

$$\tilde{\mathbf{P}}_{\text{inf}} = \boldsymbol{\sigma}, \quad \tilde{\mathbf{U}}_{\text{inf}} = \mathbf{I} + \tilde{\boldsymbol{\varepsilon}}, \quad (\tilde{\mathbf{U}}^{-\top})_{\text{inf}} = \mathbf{I} - \tilde{\boldsymbol{\varepsilon}}^\top, \quad (\ln J)_{\text{inf}} = \text{tr}\,\tilde{\boldsymbol{\varepsilon}}. \tag{44}$$

By substituting the relations from Eq. (44) into $(43)_1$ and comparing the result with (41) it follows that $k_1 = \eta + \frac{1}{2}\mu$ and $k_2 = -\eta$. Consequently, the expression for $\tilde{\mathbf{P}}$ furnishes

$$\tilde{\mathbf{P}} = (\mu + \eta)\tilde{\mathbf{U}} - \eta\tilde{\mathbf{U}}^{\top} + (\lambda \ln J - \mu)\tilde{\mathbf{U}}^{-\top}. \tag{45}$$

It is noted that Eqs. (42) and (45) are the extensions of the well-known compressible neo-Hookean material model of Simo and Pister (1984) to the micropolar continuous media. Now, from Eqs. $(43)_2$ and (45), the fourth-order tensors $\overline{\boldsymbol{\mathcal{A}}}^{(1)}$ and $\overline{\boldsymbol{\mathcal{A}}}^{(2)}$ are defined by

$$\left.\begin{aligned} \overline{\boldsymbol{\mathcal{A}}}^{(1)} = \frac{\partial^2 \Psi}{\partial \tilde{\mathbf{U}} \partial \tilde{\mathbf{U}}} = (\mu + \eta)\mathbf{I} \odot \mathbf{I} - \eta \mathbf{I} \boxtimes \mathbf{I} + \lambda \tilde{\mathbf{U}}^{-\top} \otimes \tilde{\mathbf{U}}^{-\top} + (\mu - \lambda \ln J)\tilde{\mathbf{U}}^{-\top} \boxtimes \tilde{\mathbf{U}}^{-\top} \\ \overline{\boldsymbol{\mathcal{A}}}^{(2)} = \frac{\partial^2 \Psi}{\partial \boldsymbol{\Gamma} \partial \boldsymbol{\Gamma}} = \mu l^2 \mathbf{I} \odot \mathbf{I} \end{aligned}\right\}, \tag{46}$$

where use has been made of the relation $\partial \tilde{\mathbf{U}}^{-\top} / \partial \tilde{\mathbf{U}} = -\tilde{\mathbf{U}}^{-\top} \boxtimes \tilde{\mathbf{U}}^{-\top}$. It is noted that the tensors $\overline{\boldsymbol{\mathcal{A}}}^{(1)}$ and $\overline{\boldsymbol{\mathcal{A}}}^{(2)}$ are used in Eq. (25) to calculate the components of the fourth-order tensors $\boldsymbol{\mathcal{A}}^{(1)}$ and $\boldsymbol{\mathcal{A}}^{(2)}$, respectively. Obviously, the fourth-order tensors $\boldsymbol{\mathcal{A}}^{(3)}$ and $\boldsymbol{\mathcal{A}}^{(4)}$ are identically zero in the present constitutive model.

4.5. A brief review of the theory of Zhao et al. (2019)

An elegant continuum theory for the deformation analysis of HMSMs has been developed by Zhao et al. (2019). Despite having an asymmetric Cauchy stress tensor, their theory is very similar to the classical continuum theory in the sense that it neither needs non-classical material parameters nor additional degrees of freedom. Moreover, it satisfies the angular momentum balance law identically. The main assumption is that the free energy per unit reference volume is the summation of two parts, namely the mechanical part Ψ^{mech} and the magnetic one Ψ^{mag}, namely (Zhao et al., 2019)

$$\Psi = \Psi^{\text{mech}}(\mathbf{F}) + \Psi^{\text{mag}}(\mathbf{F}, \tilde{\mathbb{B}}^{\text{r}}, \mathbb{B}^{\text{ext}}) \quad \text{with} \quad \Psi^{\text{mag}} = -\frac{1}{\mu_0}\mathbf{F}\tilde{\mathbb{B}}^{\text{r}} \cdot \mathbb{B}^{\text{ext}}. \tag{47}$$

The first Piola–Kirchhoff stress resulting from Eq. (47) is as follows:

$$\mathbf{P} = \mathbf{P}^{\text{mech}} + \mathbf{P}^{\text{mag}} \quad \text{with} \quad \mathbf{P}^{\text{mech}} = \frac{\partial \Psi^{\text{mech}}}{\partial \mathbf{F}} \quad \text{and} \quad \mathbf{P}^{\text{mag}} = \frac{\partial \Psi^{\text{mag}}}{\partial \mathbf{F}} = -\frac{1}{\mu_0}\mathbb{B}^{\text{ext}} \otimes \tilde{\mathbb{B}}^{\text{r}}. \tag{48}$$

Obviously, if $\tilde{\mathbb{B}}^{\text{r}}$ and $\mathbb{B}^{\text{ext}}$ are constant vectors, then the magnetic stress $\mathbf{P}^{\text{mag}}$ will be constant at all material points of the body. It is noted that in the traditional formulations of continuum

mechanics, the constitutive equation of stress depends only upon kinematic tensors. However, in the theory of Zhao et al. (2019), the external loading $\mathbb{B}^{\text{ext}}$ contributes directly in the internal energy density Ψ. Accordingly, the constitutive equation for the stress tensor $\mathbf{P}$ in Eq. (48) is a function of external loading besides the kinematic deformation gradient tensor $\mathbf{F}$. In other words, the work of external loads manifests itself in the stress $\mathbf{P}$, which is intrinsically an *internal quantity*. Therefore, if the magnitude and the direction of the vectors $\tilde{\mathbb{B}}^{\text{r}}$ and $\mathbb{B}^{\text{ext}}$ are constant, and if all the boundary points of the body are fixed, then the theory of Zhao et al. (2019) states that no deformation takes place in the body. This point is elaborated in the following example:

Example In one-dimensional case, as shown in Fig. 1, a hard-magnetic soft beam of the length L, the constant undeformed cross-sectional area A_0, the constant $\tilde{\mathbb{B}}^r = |\tilde{\mathbb{B}}^r|\mathbf{e}_1$, and subjected to the constant $\mathbb{B}^{\text{ext}} = |\mathbb{B}^{\text{ext}}|\mathbf{e}_3$ is considered. In this case, the shear stress component $P_{31}^{\text{mag}} = -\frac{1}{\mu_0}|\mathbb{B}^{\text{ext}}||\tilde{\mathbb{B}}^{\text{r}}|$, which is a known quantity, is obtained. After integrating over the cross-sectional area of the beam, and moving the resulting expression to the right hand side of the governing equations, an equivalent external shear force of the form

$$Q = -\int_{A_0} P_{31}^{\text{mag}} \mathrm{d}A_0 = -A_0 P_{31}^{\text{mag}} = \frac{1}{\mu_0} A_0 |\mathbb{B}^{\text{ext}}||\tilde{\mathbb{B}}^{\text{r}}| \tag{49}$$

is obtained, which is a constant quantity in this example. In other words, the magnetic part of strain energy density Ψ^{mag} generates external shear force on the beam. If the beam is decomposed into several elements, immaterial of finite or infinitesimal elements, the shear forces between two adjacent areas are in the opposite directions. Therefore, the assembled force on the beam manifests itself as the shear force $-Q$ at $X_1 = 0$ and the shear force $+Q$ at $X_1 = L$. Now, if both boundaries of the beam are fixed to move in the X_3 direction, e.g., for the case of clamped or hinged supports, no deformation in the beam is predicted by this theory. It is noted that the condition $u_3 = 0$ at both ends is a Dirichlet boundary condition while considering the shear force Q is a Neumann condition. It is impossible to have both types of conditions at a boundary point. Moreover, the theory of Zhao et al. (2019) allows for just enforcing the condition $u_3 = 0$ for the case of clamped or hinged supports. Therefore, the shear force at $X_1 = L$ cannot generate any deformation in the mentioned beams. In other words, *if* $\tilde{\mathbb{B}}^r$ *and* $\mathbb{B}^{ext}$ *are constant vectors in a straight beam, the theory of Zhao et al. (2019) works only for the case of cantilever boundary condition*. It is noted that this conclusion is independent of the method of solution, and holds

true for all analytical and numerical techniques.

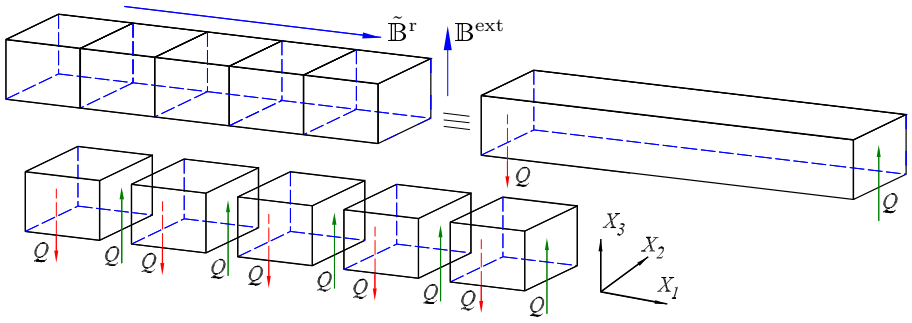

Figure 1: The magnetic shear force $Q = \frac{1}{\mu_0} A_0 |\mathbb{B}^{\mathrm{ext}}||\tilde{\mathbb{B}}^{\mathrm{r}}|$ in adjacent elements for $\tilde{\mathbb{B}}^{\mathrm{r}} = ||\tilde{\mathbb{B}}^{\mathrm{r}}||_{\mathbb{e}_1}$ and $\mathbb{B}^{\mathrm{ext}} = ||\mathbb{B}^{\mathrm{ext}}||_{\mathbb{e}_3}$

To investigate another difference between the present formulation and that of Zhao et al. (2019), suppose that both $\tilde{\mathbb{B}}^{\mathrm{r}}$ and $\mathbb{B}^{\mathrm{ext}}$ are in the same directions. For instance, similar to Fig. 1, consider a rod in the X_1-direction. Let $\tilde{\mathbb{B}}^{\mathrm{r}} = |\tilde{\mathbb{B}}^{\mathrm{r}}|\mathbf{e}_1$ and $\mathbb{B}^{\mathrm{ext}} = |\mathbb{B}^{\mathrm{ext}}|\mathbf{e}_1$ be along the length of the rod. In this case, from Eq. $(48)_3$, the magnetic stress component $P_{11}^{\mathrm{mag}} = -|\tilde{\mathbb{B}}^{\mathrm{r}}||\mathbb{B}^{\mathrm{ext}}|/\mu_0$ is obtained, which can cause axial extension in the rod. This is because the known force $P_{11}^{\mathrm{mag}} A_0$ goes to the right-hand side of the governing equation and plays the role of an extensional force on the rod. On the other hand, the magnetic body couple $\mathbb{c}^\star$ is zero in this case, because the internal and external magnetic fluxes are parallel to each other. In other words, according to the present formulation, which has been constructed based upon the cross product $(\mathbf{F}\tilde{\mathbb{B}}^{\mathrm{r}}) \times \mathbb{B}^{\mathrm{ext}}$, no deformation occurs in the rod. Zhao et al. (2019) have solved this problem numerically as well as analytically based on their model to validate the accuracy of their FE formulation. Since reliable experimental data are not available yet, it is not possible to validate or reject the results predicted by the two formulations in the mentioned problem. However, it is obvious that the two formulations lead to completely different responses.

5. Numerical examples

In this section, several examples are solved to examine the performance of the developed formulation. To do so, a home-written FE code based on the formulation presented in the previous sections has been developed. In all simulations, three-dimensional cubic elements with

20 nodes are employed. All 20 nodes of the element have displacement DOFs, and the eight nodes located at the corners of the element have rotational DOFs, as well. A standard $2 \times 2 \times 2$ Gauss integration rule has been employed to evaluate all integrals. Moreover, in all examples, the value of Poisson's ratio is considered to be $\nu = 0.48$.

5.1. Bending of cantilever beams

In this example, the elastic bending of four cantilever beams made of HMSMs and subject to an external magnetic flux is investigated. This example has been previously studied, both numerically and experimentally, by Zhao et al. (2019). The length and height of the beams are given by the sets $L \in \{11, 19.2, 17.2, 17.2\}$ (mm) and $h \in \{1.1, 1.1, 0.84, 0.42\}$ (mm), respectively. Accordingly, the aspect ratio "$AR = L/h$" of the beams will be $AR \in \{10, 17.5, 20.5, 41\}$. The width of all beams is 5 mm. Following Zhao et al. (2019), the shear modulus is considered to be $\mu = 303$ (kPa). The referential residual magnetic flux density is along the undeformed centreline and is of the form $\tilde{\mathbb{B}}^{\mathrm{r}} = 0.143\ \mathbb{e}_1$ (T). The beams are subjected to the external magnetic flux density $\mathbb{B}^{\mathrm{ext}} = 0.05\mathbb{e}_3$ (T) perpendicular to the undeformed centreline. The tip deflection of the beams is calculated for various values of the micropolar parameters η and l, and the results are compared with the data reported by Zhao et al. (2019). Numerical simulations reveal that for $\eta = 0.1\mu$ and $l = 0.1h$, with μ and h as, respectively, the shear modulus and the thickness of the beams, the present results are in good agreement with the available data. It is noted that the relations $\eta = 0.1\mu$ and $l = 0.1h$ will be also used for the next examples in this present work.

Variation of the nondimensional tip deflection u_3^{TIP}/L against the nondimensional load parameter $\frac{1}{\mu\mu_0}|\mathbb{B}^{\mathrm{ext}}||\tilde{\mathbb{B}}^{\mathrm{r}}| \times 10^3$ is displayed in Fig. 2(**a**). It is observed that the results based on the present formulation are in good agreement with the experimental and numerical data obtained by Zhao et al. (2019). The final deformed shapes of the beams are demonstrated in Fig. 2(**b**). The maximum tip deflection at the four beams is given by the set $u_{3\max}^{\mathrm{TIP}} \in \{8.18, 16.61, 15.24, 16.26\}$ (mm).

5.2. An H-shaped geometry under magnetic loading

In this example, the large deformation of an initially-flat H-shaped geometry is investigated. The geometry is composed of 15 cubic blocks of dimensions $6 \times 6 \times 0.9$ (mm) as displayed in Fig. 3(**a**). The blocks are welded together by the procedure elaborated in Kuang et al.

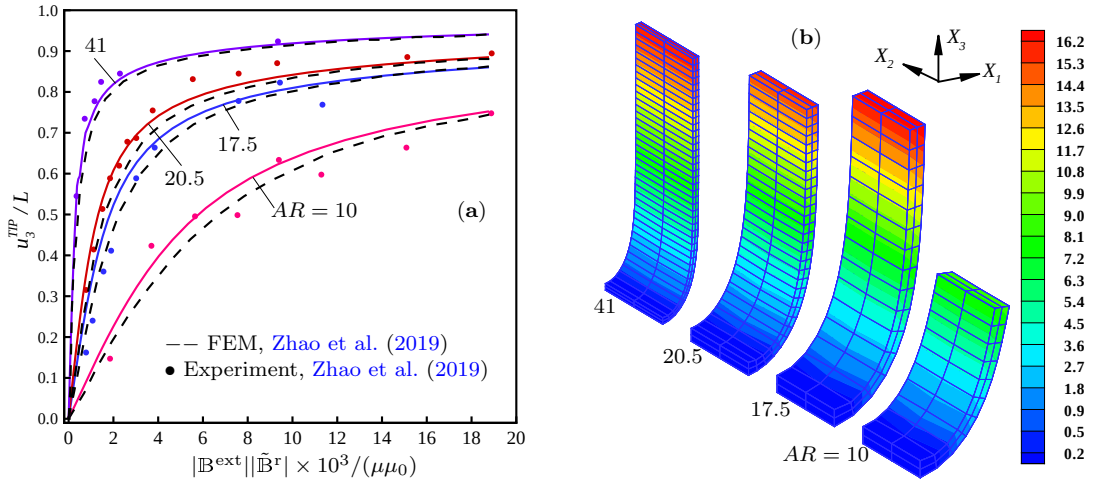

Figure 2: Cantilever beams with $\tilde{\mathbb{B}}^r = 0.143\mathbb{e}_1$ (T) under the magnetic flux $\mathbb{B}^{ext} = 0.05\mathbb{e}_2$ (T), (a): load-deflection curves, (b): final deformed shapes with the contour plots of u_3

(2021). Therefore, the overall dimensions of the geometry in the X_1X_2 plane is 42×30 (mm), and the thickness is $h = 0.9$ (mm). Following Kuang et al. (2021), the shear modulus is considered to be $\mu = 135$ (kPa). The magnitude of the referential residual magnetic flux density is $|\tilde{\mathbb{B}}^r| = 0.094$ (T). However, the direction of $\tilde{\mathbb{B}}^r$ is not constant and has been shown by the arrows on the geometry. The external magnetic flux density $\mathbb{B}^{ext} = -0.05\mathbb{e}_3$ (T) is applied to the body. Due to symmetry, it is sufficient just to discretize one-quarter of the geometry. The displacement component u_3 for several material points versus the nondimensional loading parameter $|\mathbb{B}^{ext}||\tilde{\mathbb{B}}^r| \times 10^3/(\mu\mu_0)$ is displayed in Fig. 3(**a**). The maximum lateral displacement of about 24.7 mm at the material point A is observed. Moreover, the final deformed shape of the body is illustrated in Fig. 3(**b**), which is qualitatively in agreement with the experiment of Kuang et al. (2021) in Fig. 3(**c**).

5.3. An square annuls under magnetic loading

In this example, the deformation of a square annulus geometry is investigated. The geometry is composed of 12 cubic blocks as displayed in Fig. 4(**a**). The block dimensions and material properties are the same as those given in the previous example. The external magnetic flux density $\mathbb{B}^{ext} = -0.1\mathbb{e}_3$ (T) is applied to the body. Due to rotational symmetry around the X_3-axis, one-quarter of the geometry is discretized. Fig. 4(**a**) displays the displacement component u_3 for several material points against the nondimensional loading parameter $|\mathbb{B}^{ext}||\tilde{\mathbb{B}}^r| \times 10^3/(\mu\mu_0)$. It

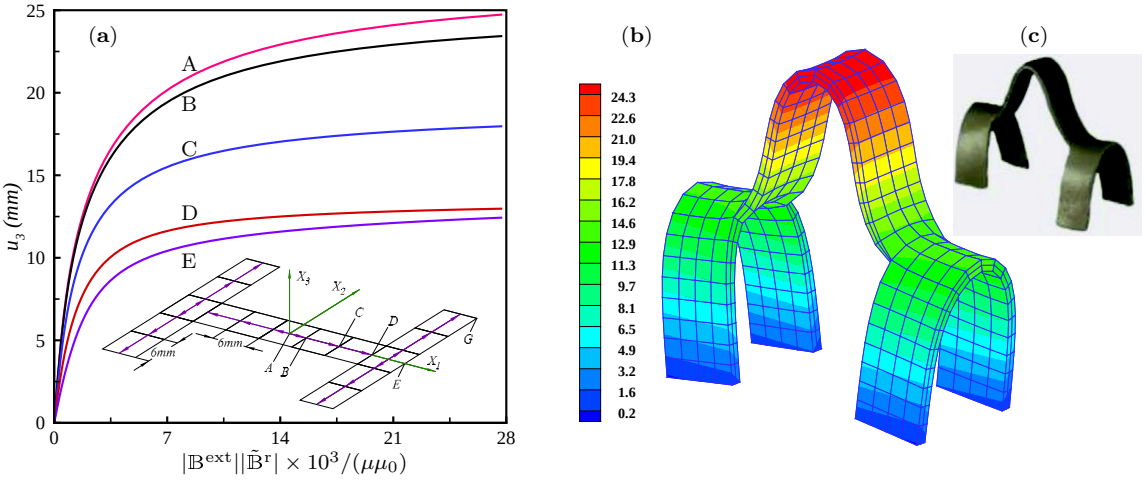

Figure 3: Deformation of an H-shaped geometry, (a): lateral deflection u_3 at some material points, (b): deformed shape with the contour plot of u_3, (c): experiment (Kuang et al., 2021)

is noted that the lateral deflection at the material point B, located at the distance 7 mm from the point A in Fig. 4(**a**) is zero. In other words, all lateral deflections are calculated relative to the point B. The maximum lateral displacement of about 3.5 mm at the material point D is observed, where the distance between D and the corner point C is 4.5 mm. The final deformed shape of the body is demonstrated in Fig. 4(**b**). The present result is qualitatively in agreement with the deformed shape in Fig. 4(**c**), obtained in the experiments of Kuang et al. (2021).

5.4. A cross-shaped geometry under magnetic loading

The large deformation of a cross-shaped body is studied in this example. As shown in Fig. 5(**a**), the geometry is composed of 9 cubic blocks. The block dimensions and material properties are the same as those in the previous two examples. The external magnetic flux density $\mathbb{B}^{\text{ext}} = 0.04\mathbb{e}_3$ (T) is applied to the body. Due to symmetry in the X_1X_2 plane, it is sufficient to discretize one-quarter of the geometry. Variations of the displacement component u_3 for several material points versus the nondimensional loading parameter $|\mathbb{B}^{\text{ext}}||\tilde{\mathbb{B}}^{\text{r}}| \times 10^3/(\mu\mu_0)$ is displayed in Fig. 5(**a**). The maximum lateral displacement of about 22.8 mm at the material point A is observed. The final deformed shape of the body is demonstrated in Fig. 5(**b**), which is qualitatively very similar to the experiment conducted by Kuang et al. (2021) and displayed in Fig. 5(**c**).

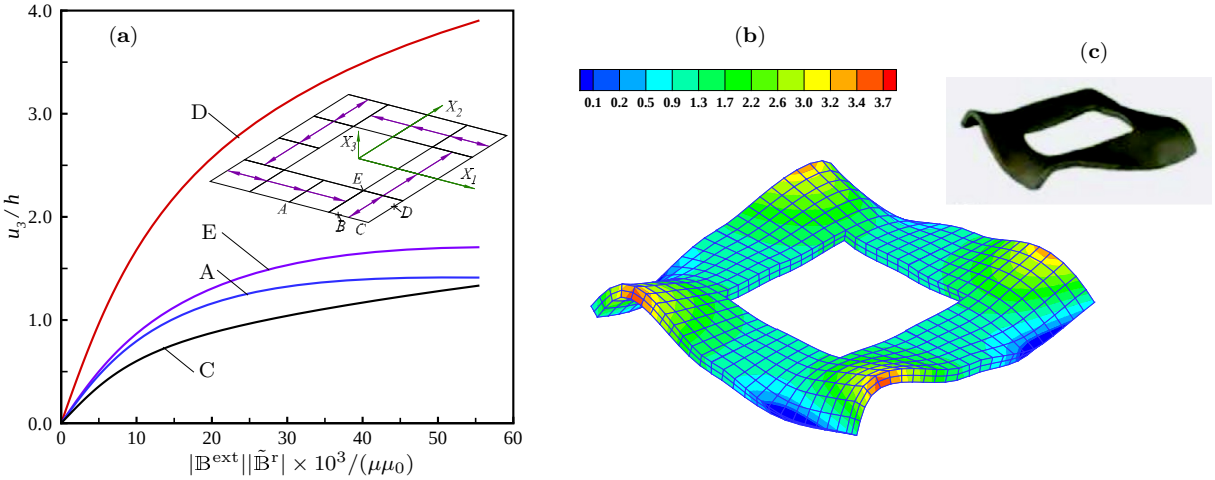

Figure 4: Deformation of an square annuls geometry, (a): the nondimensional lateral deflection u_3/h at some material points, (b): deformed shape with the contour plot of u_3, (c): experiment (Kuang et al., 2021)

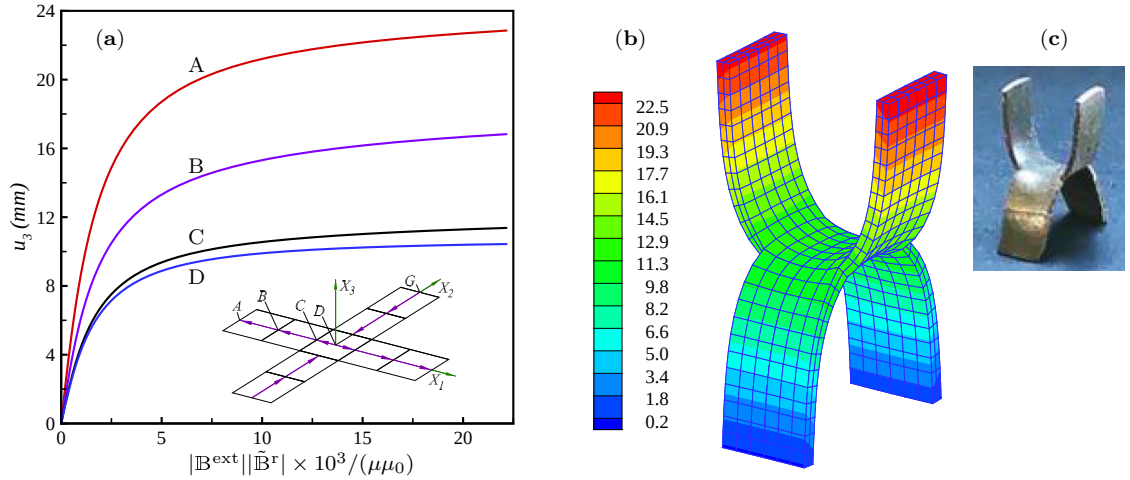

Figure 5: Deformation of a cross-shaped geometry, (a): lateral deflection u_3 at some material points, (b): final deformed shape with the contour plot of u_3, (c): experiment (Kuang et al., 2021)

5.5. Buckling of hard-magnetic soft beams under magnetic loading

The purpose of this example is to show that, in contrast to the theory of Zhao et al. (2019), the present micropolar formulation can capture the deformation of structures even if the boundaries are fixed to move in the desired direction. It is known that the application of magnetic loading on the structures made of magnetically soft materials, depending on the directions of the external magnetic induction and internal magnetization vectors, can cause the buckling of the structure (e.g., Moon and Pao (1968), and van de Ven (1978)). In this example, the beams with the aspect ratios $AR = 20.5$ and $AR = 41$, as introduced in the first example, are considered. All mechanical and magnetic properties are the same as those mentioned previously. The only difference is that two new boundary conditions, namely clamped-clamped (CC) and clamped-simply supported (CS) are considered, and the buckling behavior of the beams under a magnetic loading of the form $\mathbb{B}^{\text{ext}} = |\mathbb{B}^{\text{ext}}|\mathbb{e}_3$ is investigated. From the computational point of view, the buckling occurs when the assembled stiffness matrix of the system, after applying the boundary conditions, becomes singular. The load at which this behavior is observed is the buckling load of the beam. The maximum lateral deflection of the beams, along their centrelines, against the nondimensional loading parameter $|\mathbb{B}^{\text{ext}}||\tilde{\mathbb{B}}^{\text{r}}| \times 10^3/(\mu\mu_0)$ is depicted in Fig. 6(**a**). It is observed from the figure that, for a specific beam, and similar to the buckling under axial compressive forces, the magnetic buckling load is greater in the case of CC boundary conditions. However, as usual, the lateral deflection for the case of CS boundaries is always greater than that of the CC ones. The deformed shapes of the beam centrelines, in nondimensionalized form, are illustrated in Fig. 6(**b**). It is noted that the deformed shapes for the case of CC and CS boundary conditions are completely different. For the case of CC boundaries, the deformation is skew-symmetric with respect to the line $x_1 = L/2$. However, for CS conditions, the deformed shape is asymmetric.

6. Summary

In this work, a nonlinear formulation for finite deformation analysis of three-dimensional continuum bodies made of hard-magnetic soft materials was developed. Since the external magnetic load induces a body moment on the body, the micropolar theory was employed as the basic continuum model to capture the asymmetric property of the Cauchy stress tensor. To perform numerical solutions, variational formulation of the problem and the corresponding

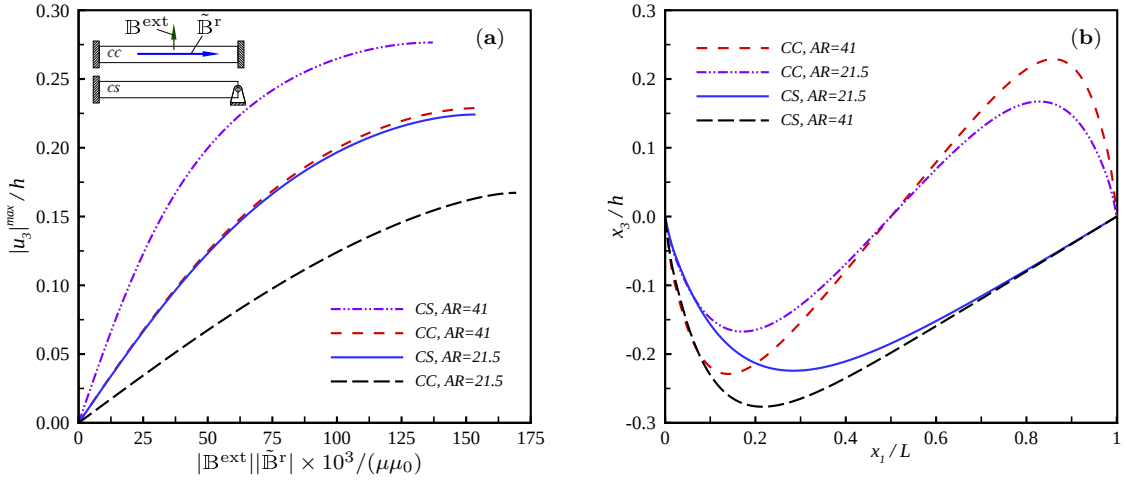

Figure 6: Buckling of two HMS beams, (a): the maximum lateral deflection $|u_3|^{\max}/h$, (b): nondimensionalized deformed shapes along the centrelines

linearization were presented. Several numerical examples were solved, and it was observed that the present formulation can capture the numerical and experimental results available in the literature. Moreover, the present formulation, in contrast to the existing theories available in the literature, can successfully predict the deformation of HMSM bodies even when the remnant magnetic induction vector is constant and the boundaries are fixed. Therefore, the present formulation is more versatile that can be used for the optimum design of devices made of HMSMs. The generalization of the present research to include viscoelastic and thermal effects will be made in the forthcoming contributions.

Declaration of competing interest

The authors declare that they have no known competing financial interests or personal relationships that could have appeared to influence the work reported in this paper.

Acknowledgements

M. Hossain acknowledges the funding through an Engineering and Physical Sciences Research Council (EPSRC) Impact Acceleration Award (EP/R511614/1). M. Hossain also acknowledges the support by EPSRC through the Supergen ORE Hub (EP/S000747/1), which awarded fund-

ing for the Flexible Fund project Submerged bi-axial fatigue analysis for flexible membrane Wave Energy Converters (FF2021-1036).

References

Alapan, Y., Karacakol, A. C., Guzelhan, S. N., Isik, I., Sitti, M., 2020. Reprogrammable shape morphing of magnetic soft machines. Sci. Adv. 6, eabc6414.

Altenbach, H., Eremeyev, V.A., 2014. Strain rate tensors and constitutive equations of inelastic micropolar materials. Int. J. Plast. 63, 3–17.

Argyris, J., 1982. An excursion into large rotations. Comput. Methods Appl. Mech. Eng. 32, 85–155.

Bastola, A.K., Hossain, M., 2021. The shape-morphing performance of magnetoactive soft materials. Mat. Des. 211,110172.

Bauer, S., Schäfer, M., Grammenoudis, P., Tsakmakis. C., 2010. Three-dimensional finite elements for large deformation micropolar elasticity. Comput. Methods Appl. Mech. Eng. 199, 2643–2654.

Bauer, S., Dettmer, W.G., Peric, D., Schäfer, M., 2012b. Micropolar hyper-elastoplasticity: constitutive model, consistent linearization, and simulation of 3D scale effects. Int. J. Numer. Meth. Eng. 91, 39–66.

Bauer, S., Dettmer, W.G., Peric, D., Schäfer, M., 2012b. Micropolar hyper-elasticity: constitutive model, consistent linearization and simulation of 3D scale effects. Comput. Mech. 50, 383–396.

Bica, I., 2012. The influence of the magnetic field on the elastic properties of anisotropic magnetorheological elastomers. J. Ind. Eng. Chem. 18, 1666–1669.

Boczkowska, A., Awietjan, S.F., 2009. Smart composites of urethane elastomers with carbonyl iron. J. Mater. Sci. 44, 4104–4111.

Böse, H., 2007. Viscoelastic properties of silicon-based magnetorheological elastomers, Int. J. Mod. Phys. B 21, 4790–4797.

Bustamante, R., Shariff, M.H.B.M., Hossain, M., 2021. Mathematical formulations for elastic magneto-electrically coupled soft materials at finite strains: Time-independent processes. Int. J. Eng. Sci. 159, 103429.

Chen, W., Wang, L., 2020. Theoretical modeling and exact solution for extreme bending deformation of hard-magnetic soft beams. J. Appl. Mech. 87, 041002.

Chen, W., Yan, Z., Wang, L., 2020a. Complex transformations of hard-magnetic soft beams by designing residual magnetic flux density. Soft Matter 16, 6379–6388.

Chen, W., Yan, Z., Wang, L., 2020b. On mechanics of functionally graded hard-magnetic soft beams. Int. J. Eng. Sci. 157, 103391.

Chen, W., Wang, L., Yan, Z., Luo, B., 2021. Three-dimensional large-deformation model of hard-magnetic soft beams. Compos. Struct. 266, 113822.

Chowdhury, S.R., Rahaman, M.M., Roy, D., Sundaram, N., 2015. A micropolar peridynamic theory in linear elasticity. Int. J. Solids Struct. 59, 171–182.

de Borst, R., 1993. A generalization of J_2-flow theory for polar continua. 103, 347–362.

Dorfmann, A., Ogden, R.W., 2004. Nonlinear magnetoelastic deformations of elastomers. Acta Mech. 167, 13–28.

Dorfmann, A., Ogden, R.W., 2014. Nonlinear Theory of Electroelastic and Magnetoelastic Interactions. Springer.

Erdelj, S.G., Jelenić, G., Ibrahimbegović, A., 2020. Geometrically non-linear 3D finite-element analysis of micropolar continuum. Int. J. Solids Struct. 202, 745–764.

Eringen, A.C., 1999. Microcontinuum Field Theories, vol. I, Foundations and Solids. Springer.

Eringen, A.C., Kafadar, C.B., 1976. Polar field theories. In: Eringen, A.C. (Ed.), Continuum Physics, vol. IV. Academic Press, pp. 1–73.

Ethiraj, G., Miehe, C., 2016. Multiplicative magneto-elasticity of magnetosensitive polymers incorporating micromechanically-based network kernels. Int. J. Eng. Sci. 102, 93–119.

Garcia-Gonzalez, D., 2019. Magneto-visco-hyperelasticity for hard-magnetic soft materials: theory and numerical applications. Smart Mater. Struct. 28, 085020.

Garcia-Gonzalez, D., Hossain, M., 2021a. A microstructural-based approach to model magneto-viscoelastic materials at finite strains. Int. J. Solids Struct. 208–209, 119–132.

Garcia-Gonzalez, D., Hossain, M., 2021b. Microstructural modelling of hard-magnetic soft materials: Dipole–dipole interactions versus Zeeman effect. Extreme Mech. Lett. 48, 101382.

Goda, I., Assidi, M., Ganghoffer, G.F., 2014. A 3D elastic micropolar model of vertebral trabecular bone from lattice homogenization of the bone microstructure. Biomech. Model. Mechanobiol. 13, 53–83.

Grammenoudis, P., Tsakmakis, C., 2001. Hardening rules for finite deformation micropolar plasticity: Restrictions imposed by the second law of thermodynamics and the postulate of Iliushin. Cont. Mech. Thermodyn. 13, 325–363.

Grammenoudis, P., Tsakmakis, C., 2007. Micropolar plasticity theories and their classical limits. Part I: Resulting model. Acta Mech. 189, 151–175.

Grammenoudis, P., Sator, C., Tsakmakis, C., 2007. Micropolar plasticity theories and their classical limits. Part II: Comparison of responses predicted by the limiting and a standard classical model. Acta Mech. 189, 177–191.

Hu, W., Zhan, G., Mastrangeli, M., Sitti, M., 2018. Small-scale soft-bodied robot with multimodal locomotion. Nature 554, 81–85.

Iordache, M.-M., Willam, K., 1998. Localization failure analysis in elastoplastic Cosserat continua. Comput. Methods Appl. Mech. Eng. 151, 559–586.

Hu, X., Zhu, H., Chen, S., Yu, H., Qu, S., 2022. Magnetomechanical behavior of soft magnetoactive membranes. Int. J. Solids Struct. 234–235, 111310.

Ivaneyko, D., Toshchevikov, V., Saphiannikova, M., Heinrich, G., 2012. Effects of particle distribution on mechanical properties of magneto-sensitive elastomers in a homogeneous magnetic field. Condens. Matter Phys. 15, 33601.

Kafadar, C.B., Eringen, A.C., 1971. Micropolar media–I the classical theory. Int. J. Eng. Sci. 9 (3), 271–307.

Kalina, K.A., Brummund, J., Metsch, P., Kaestner, M., Borin, D.Y., Linke, J.M., Odenbach, S., 2017. Modeling of magnetic hystereses in soft MREs filled with NdFeB particles. Smart Mater. Struct. 26, 105019.

Kim, Y., Yuk, H., Zhao, R., Chester, S.A., Zhao, X., 2018. Printing ferromagnetic domains for untethered fast-transforming soft materials. Nature 558, 274–279.

Kuang, X., Wu, S., Ze, Q., Yue, L., Jin, Y., Montgomery, S.M., Yang, F., Qi, H.J., Zhao, R., 2019. Magnetic dynamic polymers for modular assembling and reconfigurable morphing architectures. Adv. Mater. 2102113.

Lee, M., Park, T., Kim, C., Park, S.M., 2020. Characterization of a magneto-active membrane actuator comprising hard magnetic particles with varying crosslinking degrees. Mater. Des. 195, 108921.

Lucarini, S., Hossain, M., Garcia-Gonzalez, D.. 2022. Recent advances in hard-magnetic soft composites: synthesis, characterisation, computational modelling, and applications. Compos. Struct. 200, 210001.

Lum, G.Z., Ye, Z., Dong, X., Marvi, H., Erin, O., Hu, W., Sitti, M., 2016. Shape-programmable magnetic soft matter. Proc. Natl. Acad. Sci. 113, E6007–E6015.

Mayeur, J.R., McDowell, D.L., Bammann, D.J., 2011. Dislocation-based micropolar single crystal plasticity: Comparison of multi- and single criterion theories. J. Mech. Phys. Solids 59, 398–422.

Mehnert, M., Hossain, M., Steinmann, P., 2017. Towards a thermo-magneto-mechanical coupling framework for magneto-rheological elastomers. Int. J. Solids Struct. 128, 117–132.

Moon, F.C., Pao, Y.W., 1968. Magnetoelastic buckling of a thin plate. J. Appl. Mech. 35, 53–58.

Mukherjee, D., Bodelot, L., Danas, K., 2020. Microstructurally-guided explicit continuum models for isotropic magnetorheological elastomers with iron particles. Int. J. Non-Linear Mech. 120, 103380.

Mukherjee, D., Rambausek, M., Danas, K., 2021. An explicit dissipative model for isotropic hard magnetorheological elastomers. J. Mech. Phys. Solids 151, 104361.

Pietraszkiewicz, W., Eremeyev, V.A., 2009. On natural strain measures of the non-linear micropolar continuum. Int. J. Solids Struct. 46, 774–787.

Rajan, A., Arockiarajan, A., 2021. Bending of hard-magnetic soft beams: A finite elasticity approach with anticlastic bending. Eur. J. Mech. A Solids 90, 104374.

Ramezani, S., Naghdabadi, R., 2007. Energy pairs in the micropolar continuum. Int. J. Solids Struct. 44, 4810–4818.

Ramezani, S., Naghdabadi, R., Sohrabpour, S., 2008. Non-linear finite element implementation of micropolar hypo-elastic materials. Comput. Methods Appl. Mech. Eng. 197, 4149–4159.

Ramezani, S., Naghdabadi, R., Sohrabpour, S., 2009. Constitutive equations for micropolar hyper-elastic materials. Int. J. Solids Struct. 46, 2765–2773.

Ren, Z., Hu, W., Dong, X., Sitti, M., 2019. Multi-functional soft-bodied jellyfish-like swimming. Nature Commun. 10, 2703.

Sano, T.G., Pezzulla, M., Reis, P.M., 2021. A Kirchhoff-like theory for hard magnetic rods under geometrically nonlinear deformation in three dimensions. *arXiv*:2106.15189.

Saxena, P., Hossain, M., Steinmann, P., 2013. A theory of finite deformation magneto-viscoelasticity. Int. J. Solids Struct. 50, 3886–3897.

Schümann, M., Borin, D.Y., Huang, S., Auernhammer, G.K., Müller, R., Odenbach, S., 2017. A characterisation of the magnetically induced movement of NdFeB-particles in magnetorheological elastomers. Smart Mater. Struct. 26, 095018.

Schümann, M., Borin, D.Y., Morich, J., Odenbach, S., 2020. Reversible and non-reversible motion of NdFeB-particles in magnetorheological elastomers. J. Intell. Mater. Syst. Struct. 32, 3–15.

Simo, J.C., Pister, K.S., 1984. Remarks on rate constitutive equation for finite deformation problems: computational implications. Comput. Methods Appl. Mech. Eng. 46, 201–215.

Spadoni, A., Ruzzene, M., 2012. Elasto-static micropolar behavior of a chiral auxetic lattice. J. Mech. Phys. Solids 60, 156–171.

Steinmann, P., Willam, K., 1991. Localization within the framework of micropolar elastoplasticity. In: Advances in continuum mechanics (Bruller, O., Mannl, V., Najar, J. Eds). Springer, Berlin.

Steinmann, P., 1994. A micropolar theory of finite deformation and finite rotation multiplicative elastoplasticity. Int. J. Solids Struct. 31 (8), 1063–1084.

Suh, S.S., Sun, W-C., OConnor, D.T., 2020. A phase field model for cohesive fracture in micropolar continua. Comput. Methods Appl. Mech. Eng. 369, 113181.

Tejchman, J., Wu., W., 2007. Modeling of textural anisotropy in granular materials with stochastic micropolar hypoplasticity. Int. J. Non-Linear Mech. 42, 882–894.

van de Ven, A.A.F., 1978. Magnetoelastic buckling of thin plates in a uniform transverse magnetic field. J. Elast. 8, 297–312.

Wang, L., Kim, Y., Guo, G.F., Zhao, X., 2020. Hard-magnetic elastica. J. Mech. Phys. Solids 142, 104045.

Wang, L., Zheng, D., Harker, P., Patel, A.B., Guo, C.F., Zhao, X., 2021. Evolutionary design of magnetic soft continuum robots. Proc. Natl. Acad. Sci. 118, 21.

Wriggers, P., 2008. Nonlinear Finite Element Methods. Springer.

Wu, S., Ze, Q., Zhang, R., Hu, N., Cheng, Y., Yang F., Zhao, R., 2019. Symmetry-breaking actuation mechanism for soft robotics and active metamaterials. ACS Appl. Mater. Interfaces 11, 41649–41658.

Wu, S., Hamel, C.M., Ze, Q., Yang, F., Qi, H.J., Zhao, R., 2021. Evolutionary algorithm-guided voxel-encoding printing of functional hard-magnetic soft active materials. Adv. Intell. Syst. 2, 2000060.

Wu, S., Hu, W., Ze, Q., Sitti, M., Zhao, R., 2020. Multifunctional magnetic soft composites: a review. Multifuct. Mater. 3, 042003.

Yan, D., Abbasi, A., Reis, P.M., 2021. A comprehensive framework for hard-magnetic beams: reduced-order theory, 3D simulations, and experiments. Int. J. Solids Struct. https://doi.org/10.1016/j.ijsolstr.2021.111319.

Yarali, E., Banishadi, M., Zolfagharian, A., Chavoshi, M., Arefi, F., Hossain, M., Bastola, A., Ansari, M., Foyouzat, A., Dabbagh, A., Ebrahimi, M., Mirzaali, M. J., Bodaghi, M. Magneto/ electroresponsive polymers toward manufacturing, characterization, and biomedical/ soft robotic applications. Appl. Mater. Today. 26, 101306.

Ye, H., Li, Y., Zhang, T., 2021. Magttice: A lattice model for hard-magnetic soft materials. Soft Matter 17, 3560–3568.

Yoder, M., Thompson, L., Summers, J., 2018. Size effects in lattice structures and a comparison to micropolar elasticity. Int. J. Solids Struct. 143, 245–261.

Yu, H., Chen, X., 2021. A viscoelastic micropolar peridynamic model for quasi-brittle materials incorporating loading-rate effects. Comput. Methods Appl. Mech. Eng. 383, 113897.

Zabihyan, R., Mergheim, J., Pelteret, J.P., Brands, B., Steinmann, P., 2020. FE^2 simulations of magnetorheological elastomers: influence of microscopic boundary conditions, microstructures and free space on the macroscopic responses of MREs. Int. J. Solids Struct. 193, 338–356.

Guarín-Zapata, N., Gomez, J., Valencia, C., Dargush, G.F., Hadjesfandiari, A.R., 2020. Finite element modeling of micropolar-based phononic crystals. Wave Motion 92, 102406.

Zhang, R. Wu, S. Qiji, Z., Zhao, Z., 2020. Micromechanics study on actuation efficiency of hard-magnetic soft active materials. 87, 091008.

Zhao, R., Kim, Y., Chester, A.S., Sharma, P., Zhao, X., 2019. Mechanics of hard-magnetic soft materials. J. Mech. Phys. Solids 124, 244–263.